Preprint
UCRL-JC-147395

Theoretical Model and Interpretation of X-Ray Thomson Scattering Measurements in Warm Dense Matter

G. Gregori, S.H. Glenzer, O.L. Landen, R.W. Lee

This article was submitted to
13th American Physical Society Topical Conference on Atomic Processes in Plasmas, Gatlinburg, Tennessee, April 22-25, 2002

April 3, 2002

U.S. Department of Energy

Lawrence Livermore National Laboratory

Theoretical model and interpretation of x-ray Thomson scattering measurements in warm dense matter

G. Gregori, S. H. Glenzer, O. L. Landen, and R. W. Lee

Lawrence Livermore National Laboratory, University of California, P.O. Box 808, CA 94551

(April 3, 2002)

Abstract

We present analytical expressions for the dynamic structure factor, or form factor $S(k,\omega)$, which is the quantity describing the inelastic x-ray cross section from a dense plasma or a simple liquid. Our results, based on the random phase approximation (RPA) for the treatment on the charged particle coupling, can be applied to describe scattering from either weakly coupled classical plasmas or degenerate electron liquids. Our form factor correctly reproduces the Compton energy downshift and the usual Fermi-Dirac electron velocity distribution for $S(k,\omega)$ in the case of a cold degenerate plasma. The usual concept of scattering parameter is also reinterpreted for the degenerate case in order to include the effect of the Thomas-Fermi screening. The results shown in this work can be applied to interpreting x-ray scattering in warm dense plasmas occurring in inertial confinement fusion experiments or inside the interior of planets .

I. INTRODUCTION

Diagnostics of dense plasmas poses several difficulties as currently adopted experimental techniques are rather limited in probing particle densities, temperatures and charge states of warm dense matter. Optical techniques, for example, can only provide information on surface layers of dense plasmas since they are opaque to visible or UV light. On the other hand, the emerging interest in understanding the properties of matter under extreme conditions, as the ones achieved in inertial confinement fusion (ICF) experiments [1], necessitates the developing of finite temperature dense matter probes. In ICF implosion experiments a variety of plasma regimes are created, and of particular interest are Fermi degenerate (or quantum) plasmas, characterized by a Fermi temperature greater than the electron kinetic temperature. Moreover, equation of state (EOS) predictions for various degenerate plasmas can only be resolved by accurate measurements of the chemical state of the materials. However, uncertainties in the present data and the lack of reliable independent measurements of temperature and density have prevented validation of current models and calculations.

We investigate the possibility of extending spectrally resolved Thomson scattering [2] in the x-ray regime for the diagnostics of solid density plasmas. This method was first discussed by Landen *et al.* [3] as a viable diagnostics alternative in ICF experiments. In Ref. [3], calculations were presented for scattering parameters $\alpha = 1/k\lambda_D \ll 1$, where λ_D is the Debye length and $\mathbf{k} = \mathbf{k}_0 - \mathbf{k}_1$ is the difference between the wave-number of the scattered and the incident probe radiation. In the present work, we provide a theoretical expression for the scattering form factor to represent x-ray Thomson scattering for arbitrary α parameter. In addition, our treatment can be applied in the description of scattering from degenerate to weakly coupled plasmas. For plasmas obeying the classical statistics, the electron-electron coupling constant is defined as (see, *e.g.,* Ichimaru [4]) $\Gamma = e^2/4\pi\epsilon_0 k_B T_e d$, where T_e is the electron temperature and $d = (3/4\pi n_e)^{1/3}$ the ion-sphere radius, with n_e the electron density. In other words, Γ is the ratio between the potential and the kinetic energy of the electrons. For coupling between different charged particles, we also need to account

for the ionization state of the material. The extension of definition of the coupling constant Γ to the quantum domain (*i.e.,* a degenerate plasma) is discussed by Liboff [5]. In this case, quantum diffraction prevents the electrons to get arbitrarily close to each other and Γ is now the ratio between the potential and the Fermi energy, E_F, of the electrons. Since $E_F = \hbar^2(3\pi^2 n_e)^{2/3}/2m_e$, as electron density increases, in contrast to a classical plasma, the coupling constant decreases.

In an ideal plasma, $\Gamma \ll 1$ and the kinetic energy dominates the particle motion with negligible inter-particle coupling, while in a strongly coupled plasma, $\Gamma \gg 1$, the electrostatic (Coulomb) forces determine the nature of the particle motion. Weakly coupled plasmas lie in the range $\Gamma \lesssim 1$. Indeed, the possibility of directly measuring temperature and ionization state in weakly and strongly coupled plasmas is of particular relevance in EOS calculation since current models predict different behavior in the material properties and an independent experimental verification would be necessary to resolve the controversy. Further discussion on the subject can be found in Landen *et al.* [3] and references therein.

II. THEORY

A. Basic definitions

We are interested in describing the scattering from a uniform plasma containing N ions per unit volume. If Z_A is the nuclear charge of the ion, the total number of electrons per unit volume in the system, including free and bound ones, is $Z_A N$. Let us now assume we probe such a system with x-ray radiation of frequency ω_0 such that $\hbar\omega_0 \gg E_I$, with E_I the ionization energy of any bound electron, *i.e.,* the incident frequency must be large compared to any natural absorption frequency of the scattering atom, which allows us to neglect photoabsorption. During the scattering process, the incident photon transfers momentum $\hbar\mathbf{k}$ and energy $\hbar\omega = \hbar\omega_0 - \hbar\omega_1$ to the electron, where ω_1 is the frequency of the scattered radiation. Under these conditions we can distinguish between electrons that are *kinemat-*

ically free with respect to the scattering process and *core* electrons that are tightly bound to the atom. If a_n is the orbital radius of the electron with principal quantum number n, kinematically free electrons satisfy the relation [6,7] $ka_n \gtrsim 1$, while the opposite inequality applies for core electrons. This condition is equivalent to assuming that $\hbar\omega$, the energy transferred to the electron by Compton scattering, is larger than its bound energy. In the non-relativistic limit ($\hbar\omega \ll \hbar\omega_0$)

$$k = |\mathbf{k}| = \frac{4\pi}{\lambda_0} \sin(\theta/2), \tag{1}$$

with λ_0 the probe wavelength and θ the scattering angle. We denote with Z_f and Z_b the number of kinematically free and core electrons, respectively. Clearly, $Z_A = Z_f + Z_b$. To avoid possible confusions, we should stress that Z_f is conceptually different from the *true* ionization state of the atom. It includes both the truly free (removed from the atom by ionization) and the valence (weakly bound) electrons; thus $Z_f = Z + Z_v$, where Z is the number of electrons removed from the atom, and Z_v is the number of valence electrons. In the limiting case of a liquid metal, $Z = 0$, and only the valence electrons need to be considered.

B. Scattering cross section

Following the approach of Chihara [8,9] the scattering cross section is described in terms of the dynamic structure factor of all the electrons in the plasma

$$\frac{d^2\sigma}{d\Omega d\omega} = \sigma_T \frac{k_1}{k_0} S(k,\omega), \tag{2}$$

where σ_T is the usual Thomson cross section and $S(k,\omega)$ is the total dynamic structure factor defined as

$$S(k,\omega) = \frac{1}{2\pi} \int e^{i\omega t} \langle \rho_e(\mathbf{k},t) \rho_e(-\mathbf{k},0) \rangle dt, \tag{3}$$

with $\langle ... \rangle$ denoting a thermal average and

$$\rho_e(\mathbf{k},t) = \sum_{s=1}^{Z_A N} \exp\left[i\mathbf{k}\cdot\mathbf{r}_s(t)\right], \tag{4}$$

is the Fourier transform of the total electron density distribution, with $\mathbf{r}_s(t)$ the time dependent position vector of the s-th electron. Assuming the system is isotropic, as in the case of interest here (liquid metals or plasmas), the dynamic structure factor depends only on the magnitude of k, not on its direction. The next step consists in separating the total density fluctuation, Eq. (4), between the free and core electron contributions, and separating the motion of the electrons from the motion of the ions. The details of procedure are given by Chihara [8,9], thus obtaining for the dynamic structure:

$$S(k,\omega) = |f_I(k) + q(k)|^2 S_{ii}(k,\omega) + Z_f S^0_{ee}(k,\omega) + Z_b \int \tilde{S}_{ce}(k,\omega-\omega')S_s(k,\omega')d\omega'. \tag{5}$$

The first term in Eq. (5) accounts for the density correlations of electrons that dynamically follow the ion motion. This includes both the core electrons, represented by the ion form factor $f_I(k)$, and the screening cloud of free (and valence) electrons that surround the ion, represented by $q(k)$. $S_{ii}(k,\omega)$ is the ion-ion density correlation function. The second term in Eq. (5) gives the contribution in the scattering from the free electrons that do not follow the ion motion. Here, $S^0_{ee}(k,\omega)$ is the high frequency part of the electron-electron correlation function [10] and it reduces to the usual electron feature [11] in the case of an optical probe. Inelastic scattering by core electrons is included in the last term of Eq. (5), which arises from correlation between the core electrons within an ion, $\tilde{S}_{ce}(k,\omega)$, modulated by the self-motion of the ions, represented by $S_s(k,\omega)$. We point out that in Eq. (5) electron-ion correlations are implicitly accounted in the first term, since, as shown by Chihara [8], the electron-ion response function can be written in terms of the ion-ion response function. We observe that the total density correlation function must obey the relation [13]

$$S(k,-\omega) = \exp(-\hbar\omega/k_B T_e)S(k,\omega), \tag{6}$$

which is a consequence of detail balance. This gives rise to asymmetry in the spectrum as we will discuss further in the next sections.

We will present simplified expressions for each term in Eq. (5). The relative importance of each term is discussed and scattering profiles for typical conditions found in experiments are obtained. The sensitivity to the various parameters is presented using LiH solid density plasmas as an example. A similar method based on the measurement of frequency-integrated (total) x-ray cross section for the diagnostics of high density plasmas was originally proposed by Nardi and co-workers [12,14,15]. While their approach was based on the determination of the static structure factor, we wish to determine the dynamic structure factor. This requires frequency resolved measurements, standard in optical Thomson scattering. The various terms in Eq. (5) provide scattering signals at different frequencies. With the available x-ray line sources, spectrometers and detectors in ICF experiments [3], we currently are able to resolve the high frequency part of the spectrum, $\omega \gtrsim kv_t$, where $v_t = (k_B T_e/m_e)^{1/2}$ is the electron thermal speed.

C. Ion correlations: the ion feature

We will present an analytical expression for the first term in Eq. (5). The ion-ion correlations reflect the thermal motion of the ions and/or the ion plasma frequency, and since we cannot currently experimentally access this low frequency part of the spectrum, we can approximate $S_{ii}(k,\omega) = S_{ii}(k)\delta(\omega)$. We thus only need to calculate the static structure factor for ion-ion correlations. We shall also observe that for typical conditions in dense plasmas for ICF experiments, the ions are always non-degenerate, since their thermal de Broglie wavelength is much smaller than the average interparticle distance. On the other hand, the electrons can exhibit some degree of degeneracy, and in the case of very cold and dense plasmas, they will obey the Fermi-Dirac distribution. Under these conditions, and within the framework of the random phase approximation (RPA), we can calculate $S_{ii}(k)$ using the semi-classical approach suggested by Arkhipov and Davletov [16], which is based on a pseudo-potential model for the interaction between charged particles to account for quantum diffraction effects (*i.e.*, the Pauli exclusion principle) and symmetry [17]. We shall

stress the point that in the limit of the RPA, strong coupling effects are not accounted for, thus limiting the model validity to plasma conditions in the range $\Gamma \lesssim 1$. Use of the RPA at larger couplings may still provide fairly accurate results if $kd \gtrsim 1$ [18,19]. In the cases studied here, the plasma are within the range of validity. However, extensions to strong coupling are possible in terms of a local field correction [20] of the dielectric response functions, but they are significantly more complex and can be obtained only through the solution of the hypernetted chain (HNC) equation [21] or molecular dynamics simulations [22]. In the limit discussed, the resultant expressions for the various static structures are thus:

$$S_{rs}(k,\omega) = \delta_{rs} - \frac{\sqrt{n_r n_s}}{k_B T_e}\Phi_{rs}(k), \tag{7}$$

where r, s=e (electrons) or i (ions), $n_e = Z_f n_i = Z_f N$ and the temperature has been assumed equal for both ions and electrons. Symmetry in the electron-ion interactions requires $S_{ei}(k) = S_{ie}(k)$. The coefficients $\Phi_{rs}(k)$ are given by

$$\Phi_{ee}(k) = \frac{e^2}{\epsilon_0 \Delta}\left[\frac{k^2}{1+k^2\lambda_{ee}^2} + k_{Di}^2\left(\frac{1}{(1+k^2\lambda_{ee}^2)(1+k^2\lambda_{ii}^2)} + \frac{1}{(1+k^2\lambda_{ei}^2)^2}\right) + A\left(k^2 + \frac{k_{Di}^2}{1+k^2\lambda_{ii}^2}\right)k^2\exp(-k^2/4b)\right], \tag{8}$$

$$\Phi_{ii}(k) = \frac{Z_f^2 e^2}{\epsilon_0 \Delta}\left[\frac{k^2}{1+k^2\lambda_{ii}^2} + k_{De}^2\left(\frac{1}{(1+k^2\lambda_{ee}^2)(1+k^2\lambda_{ii}^2)} - \frac{1}{(1+k^2\lambda_{ei}^2)^2}\right) + \frac{Ak^2k_{Di}^2}{1+k^2\lambda_{ii}^2}\exp(-k^2/4b)\right], \tag{9}$$

$$\Phi_{ei}(k) = -\frac{Z_f e^2}{\epsilon_0 \Delta}\frac{k^2}{1+k^2\lambda_{ei}^2}, \tag{10}$$

where $b = (\lambda_{ee}^2 \pi \ln 2)^{-1}$, $A = k_B T_e \ln 2\sqrt{\pi} b^{-3/2}\epsilon_0/e^2$, and

$$\Delta = k^4 + \frac{k^2k_{De}^2}{1+k^2\lambda_{ee}^2} + \frac{k^2k_{Di}^2}{1+k^2\lambda_{ii}^2} + k_{De}^2k_{Di}^2\left(\frac{1}{(1+k^2\lambda_{ee}^2)(1+k^2\lambda_{ii}^2)} - \frac{1}{(1+k^2\lambda_{ei}^2)^2}\right) + Ak^2k_{De}^2\left(k^2 + \frac{k_{Di}^2}{1+k^2\lambda_{ii}^2}\right)\exp(-k^2/4b). \tag{11}$$

The inverse of the electron and the ion Debye lengths are $k_{De} = (n_e e^2/\epsilon_0 k_B T_e)^{1/2}$ and $k_{Di} = (Z_f n_e e^2/\epsilon_0 k_B T_e)^{1/2}$, respectively. In Eqs. (8-11) the thermal de Broglie wavelength

is defined by $\lambda_{rs} = \hbar/(2\pi\mu_{rs}k_BT_e)^{1/2}$ with $\mu_{rs} = m_r m_s/(m_r + m_s)$ the reduced mass of the interacting pair. To complete the description of the first term of Eq. (5) we need to calculate the screening charge and the ionic form factor. The screening charge is given by [8,16]

$$q(k) = \frac{n_e e^2}{\epsilon_0 k^2 k_B T_e} \frac{C_{ei}(k)}{\epsilon(k,0)}, \tag{12}$$

where $\epsilon(k,0)$ is the electron permittivity at frequency $\omega = 0$, and $C_{ei}(k)$ the electron-ion direct correlation function. Using the Ornstein-Zernike relations [13] the electron-ion direct correlation is found to be

$$C_{ei}(k) = \frac{S_{ei}(k)}{S_{ee}(k)S_{ii}(k) - S_{ei}^2(k)}, \tag{13}$$

with the partial static structures given by Eq. (7). As we have mentioned, the ions behave as classical particles, thus the use of a semiclassical approach for the electron-ion direct correlation is justified. On the other hand,since the electrons may behave as a degenerate quantum fluid, the electron dielectric function needs to be calculated with the full effect of different statistics (Boltzmann or Fermi-Dirac) as we will discuss in the next section. To calculate the ionic form factor, $f_I(k)$, we follow the approach initially suggested by Heisenberg [23] and based on the Thomas-Fermi model of the atom [24]. Using the tables generated by Bewilogua [25], $f_I(k)$ is obtained as a function of Z_b and Z_f. Even if the calculation of the ionic form factor from the Thomas-Fermi theory is quite approximate, it compares reasonably well with the Hartree method [24]. We also note that in the limit $k \to 0$, $f_I(k) = Z_b$.

D. Electron correlations: the electron feature

The free electron density-density correlation function that appears in the second term of Eq. (5) can be formally obtained through the fluctuation-dissipation theorem [26]:

$$S_{ee}^0(k,\omega) = -\frac{\hbar}{1 - \exp(-\hbar\omega/k_BT_e)} \frac{\epsilon_0 k^2}{\pi e^2 n_e} \mathrm{Im}\left[\frac{1}{\epsilon(k,\omega)}\right], \tag{14}$$

where, as previously mentioned, $\epsilon(k,\omega)$ is the electron dielectric response function. In the case of an ideal classical plasma, the plasma dielectric response is simply evaluated from a perturbation expansion of the Vlasov equation [27]. The resultant form for the density correlation function is then known as the Salpeter electron feature [28]. This approach, however, fails when the electrons become degenerate or nearly degenerate as quantum effects begin to dominate. Under the assumption that interparticle interactions are weak, so that the nonlinear interaction between different density fluctuations is negligible, the dielectric function can be derived in a rather simple way, known as the random phase approximation (RPA) [29,30]. In the classical limit, it reduces to the usual Vlasov equation. Clearly, the RPA breaks down in presence of strong coupling when short-range collisions dominate the electron motion, thus its validity is typically limited by the condition $\Gamma \lesssim 1$, as we have previously mentioned. Deviations from the RPA have been reported, for example, by Vradis and Priftis [31] for scattering on solid beryllium at room temperature in the region $k \gtrsim k_c \sim \omega_p/v_F$, where ω_p is the plasma frequency and v_F is the velocity at the top of the Fermi surface. The critical wavenumber k_c corresponds to the transition between the plasmon and the quasi-particle excitation mode [30]. Scattering spectra near k_c have been observed to exhibit fine structures not explained within the framework of the RPA [31]. At those intermediate wave-numbers short-range correlations and high-order excitations need to be considered [32–34].

The RPA form of the dielectric function is (see, *e.g.,* Landau *et al.* [27])

$$\epsilon(k,\omega) = 1 - \frac{e^2}{\hbar\epsilon_0 k^2} \int \frac{f(\mathbf{p}+\hbar\mathbf{k}/2) - f(\mathbf{p}-\hbar\mathbf{k}/2)}{\mathbf{k}\cdot\mathbf{p}/m_e - \omega - i\nu} \frac{2d^3p}{(2\pi\hbar)^3}, \tag{15}$$

with $\nu \to 0^+$. The electron distribution function is specified as

$$f(\mathbf{p}) = \frac{1}{\exp\left(\frac{p^2/2m_e - \mu}{k_B T_e}\right) + 1}, \tag{16}$$

where $\mathbf{p}$ is the electron momentum and μ the chemical potential, defined by the normalization condition

$$\int f(\mathbf{p}) \frac{2d^3p}{(2\pi\hbar)^3} = n_e, \tag{17}$$

where we have accounted for both spin-state electrons. A useful fitting formula for the chemical potential that interpolates between the classical and the quantum regions is [35]

$$\frac{\mu}{k_B T_e} = -\frac{3}{2}\ln\Theta + \ln\frac{4}{3\sqrt{\pi}} + \frac{A\Theta^{-b-1} + B\Theta^{-(b+1)/2}}{1 + A\Theta^{-b}}, \tag{18}$$

with $\Theta = k_B T_e / E_F$ (E_F is the Fermi energy of the electrons), $A = 0.25945$, $B = 0.072$ and $b = 0858$. In the limit $T_e \to 0$, which corresponds to an electron gas in the ground state, the dielectric function takes the Lindhard form [30]. In the case of scattering from uncorrelated cold electrons, the form of the dynamic structure follows the electron velocity distribution function [36].

The free electron density-density correlation function is then determined by the numerical solution of the integral (15). It turns out that such an approach is also rather accurate to describe the collective behavior of the electrons in the valence band of metals [37,38], even if higher order correction beyond the RPA have been observed in some experiments [39,40]. In those cases, deviations from RPA resulted from the periodic potential of the crystal structure of the solid. In Fig. 1 we have plotted the normalized line profiles of $S^0_{ee}(k,\omega)$ calculated assuming an incident x-ray radiation $\lambda_0 = 0.26$ nm, corresponding to the Ti He-α 4.75 keV emission line, at a scattering angle $\theta = 160°$. We observe that the RPA calculation previously outlined automatically includes the effect of the Compton energy downshift in the scattered spectrum. This is not true, for example, in the Salpeter approximation since momentum transfer from the photons to the electrons is neglected there. Thus, in order to compare with the RPA, we need to translate the entire line profile an amount that corresponds to a shift of $\hbar^2 k^2 / 2m_e$ in energy. At a density of $n_e = 1.0 \times 10^{29}$ m^{-3}, the Fermi temperature is $T_F = 7.85$ eV. We indeed see that, at temperatures lower than T_F (Fig. 1a), when quantum effects are important, the Salpeter result deviates from the RPA one. On the other hand, at $T_e = 10$ eV (Fig. 1b), the Salpeter formula agrees very well with the RPA. In Fig. 1b we see that the profiles are broader than in Fig. 1a since the kinetic temperature is comparable to T_F. We shall also add that the conditions reported in Fig. 1 correspond to a small-α

scattering parameter ($\alpha = 0.33$[1]), *i.e.,* when collective effects are not important. This is the region where the formula derived by Landen *et al.* [3] for the dynamic structure is valid [41], and this is confirmed by the good agreement with the RPA lineshapes. At $T_e = 0$ eV the calculated profile of $S^0_{ee}(k,\omega)$ is parabolic for small α, while at $T_e = 10$ eV ($T_e > T_F$) the profile is gaussian. Since for small α the electrons behave as uncorrelated scatters, the transition from a parabolic to a gaussian profile, as the electron temperature is raised, corresponds to the transition from a Fermi to a Boltzmann statistics in the electron velocity distribution. Dynamic structures for collective scattering ($\alpha = 0.98$) are shown in Fig. 2, which correspond to a longer probe radiation of wavelength $\lambda_0 = 0.78$ nm (Al He-α 1.6 keV emission line), all the other conditions being the same as in Fig. 1. In both Figs. 1 and 2 we see the strong asymmetry in the line profiles resulting from the detail balance relation (6). This is evident from the discontinuity (kink) in the profiles at $\omega = 0$.

E. Core electron excitations

The last term in Eq. (5) corresponds to the density correlations of the tightly bound electrons within each single ion, and it arises from electron-hole and bound excitations of the inner core electrons. The Fermi *golden rule* in the first order perturbation theory can be used to calculate the spectrum resulting from electron-hole excitations [42,43]. As discussed by Mizuno and Omura [7] inner core electrons can be excited by the probe radiation to continuum states and the corresponding spectrum of the scattered radiation is that of a Raman-type band. Experiments of Suzuki [44] have then confirmed the existence of such type of excitation in the form of a weak band near the tail of the Compton band that is mainly determined by the excitations of the free electron gas. In contrast to the usual Compton scattering, the position of the Raman band is independent on k (or the scattering angle), with its threshold determined only by the ionization threshold of the inner K-shell of the atom.

---

[1]The correct definition of the scattering parameter will be given in section §III

The total scattering intensity of the Raman band is proportional to $Z_b - |f_I(k)|^2/Z_b$. For conditions typical in ICF experiments with Ti He-α 4.75 keV radiation the ionic form factor is close to Z_b, and since the Raman band has width comparable or larger than the Compton band [45], we can regard this type of contribution as yielding only a small background. This seems consistent with the preliminary results presented by Glenzer [46] on x-ray scattering from moderately heated beryllium targets. However, we need to keep in mind that, in highly correlated electron systems with $\Gamma > 1$, scattering from inner core bound electrons may be enhanced by plasma screening and collective effects [47].

III. THE SCATTERING PARAMETER

In the traditional optical Thomson scattering, the transition between collective and individual scattering is set by the parameter $\alpha = 1/k\lambda_D \sim (n_e/T_e)^{1/2}$. It represents the ratio of the probed density fluctuation wavelength, as defined by the experimental geometry, to the typical screening distance of the Coulomb field. For small values of α the scatterers behave essentially as free particles, while the large α regime reflects the collective nature of the motion. Hence, for classical plasmas, at a given probe frequency, the frequency distribution of the scattered light is described only by the ratio between the electron density and the electron temperature. However, in a degenerate fluid, the scattering parameter is not properly defined, since the screening distance is not given anymore by the Debye length. This point was discussed in Landen *et al.* [3], who, using *ad hoc* estimates, showed that in the degenerate region the screening distance is a function of the electron density only. As a result, the parameter α remains independent of the electron temperature and, consequently, the scattering profiles should remain approximately similar at a given electron density for any temperature less than T_F. In this section we will discuss these topics in a more rigorous way. As a starting point, we adopt the following definition for the scattering parameter:

$$\alpha = \frac{1}{ks}, \tag{19}$$

where s is the screening distance, defined through the relation [30]

$$\lim_{k\to 0} \epsilon(k,0) = 1 + \frac{\omega_p^2}{c_s^2 k^2} = 1 + \frac{1}{s^2 k^2}, \tag{20}$$

with c_s the isothermal electron sound speed. For a weakly-coupled, low density plasma, the isothermal sound speed is simply given by the thermal speed of the electrons, thus the usual Debye length is recovered: $s = \lambda_D = \sqrt{v_t/\omega_p}$. Conversely, in the case of a degenerate quantum fluid, the screening distance is given by the Thomas-Fermi relation [30] $s = \lambda_{TF} = \sqrt{2\epsilon_0 E_F/3e^2 n_e}$. In Fig. 3 we have plotted $\alpha = const.$ contours for a Ti He-α 4.75 keV radiation probe at $\theta = 160^\circ$ scattering angle. The contours have been obtained either by solving Eq. (20) for the screening distance, or by using the limiting expression for the screening lengths in the classical and quantum domains. We clearly see that, as the plasma becomes degenerate (*i.e.*, cold and dense), the scattering parameter becomes independent of the electron temperature. Thus, for degenerate fluids the form of the scattering profile depends strongly on the electron density and only weakly on the electron temperature.

IV. THOMSON SCATTERING PROFILES

Based on the theory outlined in the previous sections, we are now able to calculate the full Thomson scattering profile for x-ray probes at arbitrary scattering angle, for either classical or quantum plasmas. The only limitation is that the degree of coupling must not be too large to invalidate the limits of the RPA. We have obtained synthetic line profiles for the Ti He-α 4.75 keV radiation probe at $\theta = 160^\circ$ scattering angle. In addition, we have assumed that the probe material consists of LiH ($Z_A = 4$) at a compressed density $n_e = 4.0 \times 10^{29}$ m^{-3} ($T_F = 19.8$ eV) with $Z_f = 3$, $Z_b = 1$ or $Z_f = 3.5$, $Z_b = 0.5$ (Fig. 4). To simulate actual experimental data, the theoretical line profile from Eq. (5) has been convoluted with a Gaussian instrument function with 12.5 eV FWHM. From Fig. 4 we can see that synthetic line profiles tend to be fairly similar for $T_e \lesssim 10$ eV, while at higher electron temperatures the Compton peak resulting from electron correlations is heavily broadened. As we decrease the electron temperature, the electron fluid becomes degenerate and the scattering parameter

stays independent on the electron temperature. Hence, in this regime, the scattering profiles are only weakly dependent on a change in T_e.

The effect of the ionization state on the line profiles can be seen in Fig. 5. Here, we have plotted synthetic lineshapes for different values of Z_b (or Z_f) with $n_e = 1.0 \times 10^{29}$ m^{-3} ($T_F = 7.85$ eV) and $T_e = 1.0$ eV. At the same electron temperature, the Compton peaks shown in Fig. 5 are narrower than the ones shown in Fig. 4, since the broadening of the profile goes as $\sqrt{T_F} \sim n_e^{1/3}$. Also in Fig. 5, we clearly see large differences in the simulated lineshapes for the various Z_f. This effect then suggests that x-ray Thomson scattering can also be implemented as a diagnostics tool for the ionization state of solid density plasmas, in addition to T_e and n_e, based on the difference in the intensity between the unshifted and the Compton shifted peaks. This possibility was initially suggested by Landen *et al.* [3] since current optical techniques cannot directly measure the number of free electrons in dense plasmas. On the other hand, the ratio of the scattered intensities between the shifted and the unshifted peaks is only sensitive to Z_f which is *not* the same as Z, the true ionization state of the material. Since $Z_f \gtrsim Z$, the measure of Z_f will thus only provide an upper bound to Z, unless the number of valence electrons can be determined by other techniques. The ratio $I_e(k)/I_i(k)$ between the scattered intensity in the electron feature and in the ion feature is plotted in Fig. 6, where

$$I_e(k) = Z_f \int S^0_{ee}(k,\omega) d\omega = Z_f S^0_{ee}(k), \tag{21}$$

and,

$$I_i(k) = |f_I(k) + q(k)|^2 S_{ii}(k). \tag{22}$$

From Fig. 6 we see that the ratio $I_e(k)/I_i(k)$ is weakly dependent on n_e, but strongly on T_e. This suggests, that if the electron and the ion components can be isolated in an experiment, then Z_f can be determined rather accurately, without any rigorous assumption on the electron density.

V. SUMMARY AND CONCLUDING REMARKS

In this paper we have presented analytical expressions for the inelastic x-ray form factor that can be easily applied to interpreting scattering experiments in solid and super-solid density degenerate-to-hot plasmas. We have shown that x-ray Thomson scattering can be used as an effective diagnostic technique in plasmas produced under extreme conditions as the ones occurring in ICF experiments or to simulate conditions found in the interiors of planets, where the presently available diagnostics are not able, for example, to directly measure the electron temperature, ionization state, or electron conductivity.

Our calculation method is limited by the constraints of the RPA to coupling constants that are not too large. Extensions of the proposed approach to strongly coupled plasmas could be viable if local field corrections to the dielectric function are implemented, for example, by using the formalism initially developed by Hubbard [48]. Similarly, core electron-hole excitations, which have been neglected in the present work, could be important under different plasma conditions or scattering angles [44]. A different approach has been followed by Nardi [14] who has calculated the ionic form factor from the radial distribution function of the electrons around the atomic nucleus derived from one-component plasma (OCP) simulations. On the other hand, solutions of the HNC equation or molecular dynamics simulations are required to obtain the radial distribution function, thus limiting the practical use of the method if we want to effectively extract measurement values from experimental data.

ACKNOWLEDGMENTS

This work was performed under the auspices of the U.S. Department of Energy by the University of California Lawrence Livermore National Laboratory under Contract No. W-7405-ENG-48. We also acknowledge support from Laboratory Directed Research and Development grant No. 02-ERD-13.

FIGURES

FIG. 1. Free electron dynamic structure $S^0_{ee}(k,\omega)$ for $n_e = 1.0 \times 10^{29}$ m^{-3} at $T_e = 1$ eV (a) and $T_e = 10$ eV (b). The probe radiation is $\lambda_0 = 0.26$ nm and scattering angle $\theta = 160°$ ($\alpha = 0.33$).

FIG. 2. Free electron dynamic structure $S^0_{ee}(k,\omega)$ for $n_e = 1.0 \times 10^{29}$ m^{-3} at $T_e = 1$ eV (a) and $T_e = 10$ eV (b). The probe radiation is $\lambda_0 = 0.78$ nm and scattering angle $\theta = 160°$ ($\alpha = 0.98$).

FIG. 3. Electron density-temperature contours plot at constant α for a probe radiation $\lambda_0 = 0.26$ nm and scattering angle $\theta = 160°$. Open circles are derived from the solution of Eq. (20); solid lines are calculated from the limiting expressions for the screening length (see text).

FIG. 4. Synthetic dynamic structure $S(k,\omega)$ calculated for $Z_A = 4$ and $n_e = 4.0 \times 10^{29}$ m^{-3} ($T_F = 19.8$ eV). The probe radiation is $\lambda_0 = 0.26$ nm and scattering angle $\theta = 160°$. $Z_f = 3$ (a) and $Z_f = 3.5$ (b).

FIG. 5. Synthetic dynamic structure $S(k,\omega)$ calculated for $Z_A = 4$ and $n_e = 1.0 \times 10^{29}$ m^{-3} ($T_F = 7.85$ eV) and $T_e = 1.0$ eV. The probe radiation is $\lambda_0 = 0.26$ nm and scattering angle $\theta = 160°$.

FIG. 6. Ratio between the scattered intensity in the electron feature, $I_e(k)$, and in the ion feature, $I_i(k)$. $Z_A = 4$, the probe radiation is $\lambda_0 = 0.26$ nm and scattering angle $\theta = 160°$.

REFERENCES

[1] J. D. Lindl, *Inertial Confinement Fusion* (Springer-Verlag, New York, 1998)

[2] S. H. Glenzer, W. E. Alley, K. G. Estabrook, J. S. de Groot, M. G. Haines, J. H. Hammer, J.-P. Jadaud, B. J. MacGowan, J. D. Moody, W. Rozmus, L. J. Suter, T. L. Weiland, and E. A. Williams, Phys. Rev. Lett. **82**, 97 (1999).

[3] O. L. Landen, S. H. Glenzer, M. J. Edwards. R. W. Lee, G. W. Collins, R. C. Cauble W. W. Hsing, and B. A. Hammel, J. Quant. Spectrosc. Radiat. Transfer **71**, 465 (2001).

[4] S. Ichimaru, Rev. Mod. Phys. **54**, 1017 (1982).

[5] R. L. Liboff, J. Appl. Phys. **56**, 2530 (1984).

[6] V. A. Bushuev and R. N. Kuz'min, Usp. Fiz. Nauk bf 122, 81 (1977).

[7] Y. Mizuno and Y. Ohmura, J. Phys. Soc. Japan. **22**, 445 (1967).

[8] J. Chihara, J. Phys. F: Met. Phys. **17**, 295 (1987).

[9] J. Chihara, J. Phys.: Condens. Matter **12**, 231 (2000).

[10] S. Ichimaru, *Basic Principles of Plasma Physics* (Addison, Reading, MA, 1973).

[11] D. E. Evans and J. Katzenstein, Rep. Prog. Phys., **32**, 207 (1969).

[12] E. Nardi, Phys. rev. E **43**, 1977 (1991).

[13] J.-P. Hansen and I. R. McDonald, *Theory of Simple Liquids* (Academic, London, 2000)

[14] E. Nardi, Z. Zinamon, D. Riley, and N. C. Woolsey, Phys. Rev. E **57**, 4693 (1998).

[15] D. Riley, N. C. Woolsey, D. McSherry, I. Weaver, A. Djaoui, E. Nardi, Phys. Rev. Lett. **84**, 1704 (2000).

[16] Yu. V. Arkhipov and A. E. Davletov, Phys. Lett. A **247**, 339 (1998).

[17] M. Baus and J.-P. Hansen, Phys. Rep., **59**, 1 (1980).

[18] R. Cauble and D. B. Boercker, Phys. Rev. A **28**, 944 (1983).

[19] D. B. Boercker, R. W. Lee, and F. J. Rogers, J. Phys. B **16**, 3279 (1983).

[20] S. Ichimaru, S. Mitake, S. tanaka, and X.-Z. Yan, Phys. Rev. A **32**, 1768 (1985).

[21] D. D. Carley, Phys. Rev., **131**, 1406 (1963).

[22] J.-P. Hansen, *Molecular Dynamics Simulation of Coulomb Systems in two and three Dimensions*, in "Molecular Dynamics Simulation of Statistical Mechanical Systems" (G. Ciccotti and W. G. Hoover, eds.), vol. **97** (North-Holland, Amsterdam, 1986).

[23] W. Heisenberg, Z. Phys. **32**, 737 (1931).

[24] R. W. James, *The Optical principles of the Diffraction of X-rays* (Ox Bow press, Woodbridge, CT, 1962)

[25] L. Bewilogua, Z. Phys. **32**, 740 (1931).

[26] R. Kubo, J. Phys. Soc. Japan **12**, 570 (1957).

[27] L. D. Landau, E. M. Lifshitz, and L. P. Pitaevskii, *Physical Kinetics* (Pergamon, Oxford, 1995)

[28] E. E. Salpeter, Phys. Rev., **120**, 1528 (1960).

[29] D. Pines and D. Bohm, Phys. Rev. **85**, 338 (1952).

[30] D. Pines and P. Nozieres, *The Theory of Quantum Fluids* (Addison-Wesley, Redwood, CA, 1990)

[31] A. Vradis and G. D. Priftis, Phys. Rev. B **32**, 3556 (1985).

[32] K. Awa, H. Yasuhara, and T. Asahi, Phys. Rev. B **25**, 3670 (1982).

[33] K. Awa, H. Yasuhara, and T. Asahi, Phys. Rev. B **25**, 3687 (1982).

[34] T. K. Ng and B. Dabrowski, Phys. Rev. B **33**, 5358 (1986).

[35] S. Ichimaru, *Statistical Plasma Physics* (Addison-Wesley, Reading, MA, 1991), Vol. **2**

[36] J. W. DuMond and H. A. Kirkpatrick, Phys. Rev.**37**, 136 (1931).

[37] D. Pines, Rev. Mod. Phys. **28**,184 (1959).

[38] P. Nozieres and D. Pines, Phys. Rev. **113**, 1254 (2000)

[39] P. Eisenberger, P. M. Platzman, and K. C. Pandy, Phys. Rev. Lett. **31**, 311 (1973).

[40] P. Eisenberger and P. M. Platzman, Phys. Rev. B **13**, 934 (1976).

[41] S. Chandrasekhar, Phys. Rev. **34**, 1204 (1929).

[42] P. M. Platzman and N. Tzoar, Phys. Rev. **139**, A410 (1965).

[43] P. Eisenberger and P. M. Platzman, Phys. Rev. A **2**, 415 (1970).

[44] T. Suzuki, J. Phys. Soc. Japan **22**, 445 (1967).

[45] A. Issolah, Y. Garreau, B. Levi, abd G. Loupias, Phys. Rev. B **44**, 11029 (1991).

[46] S. H. Glenzer, Bull. American Phys. Soc. **46**, 325 (2001).

[47] M.-Y. Song, Y.-D. Jung, Phys. Plasma **8**, 2983 (2001).

[48] J. Hubbard, Proc. R. Soc. London, Ser A **243**, 336 (1957).

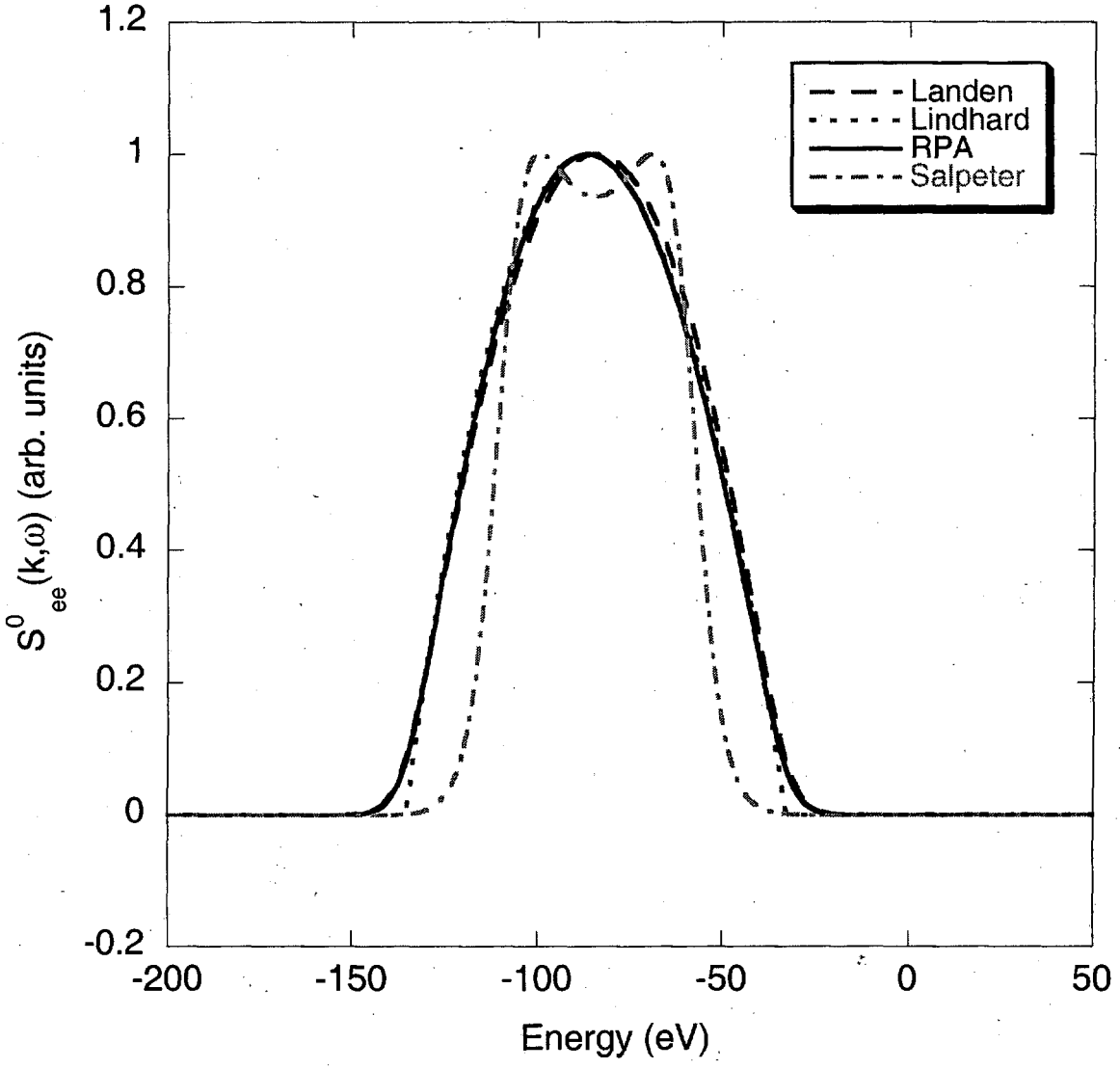
1.2
1
0.8
0.6
0.4
0.2
0
-0.2
-200
-150
-100
-50
0
50
Energy (eV)
$S^0_{ee}(k,\omega)$ (arb. units)
Landen
Lindhard
RPA
Salpeter

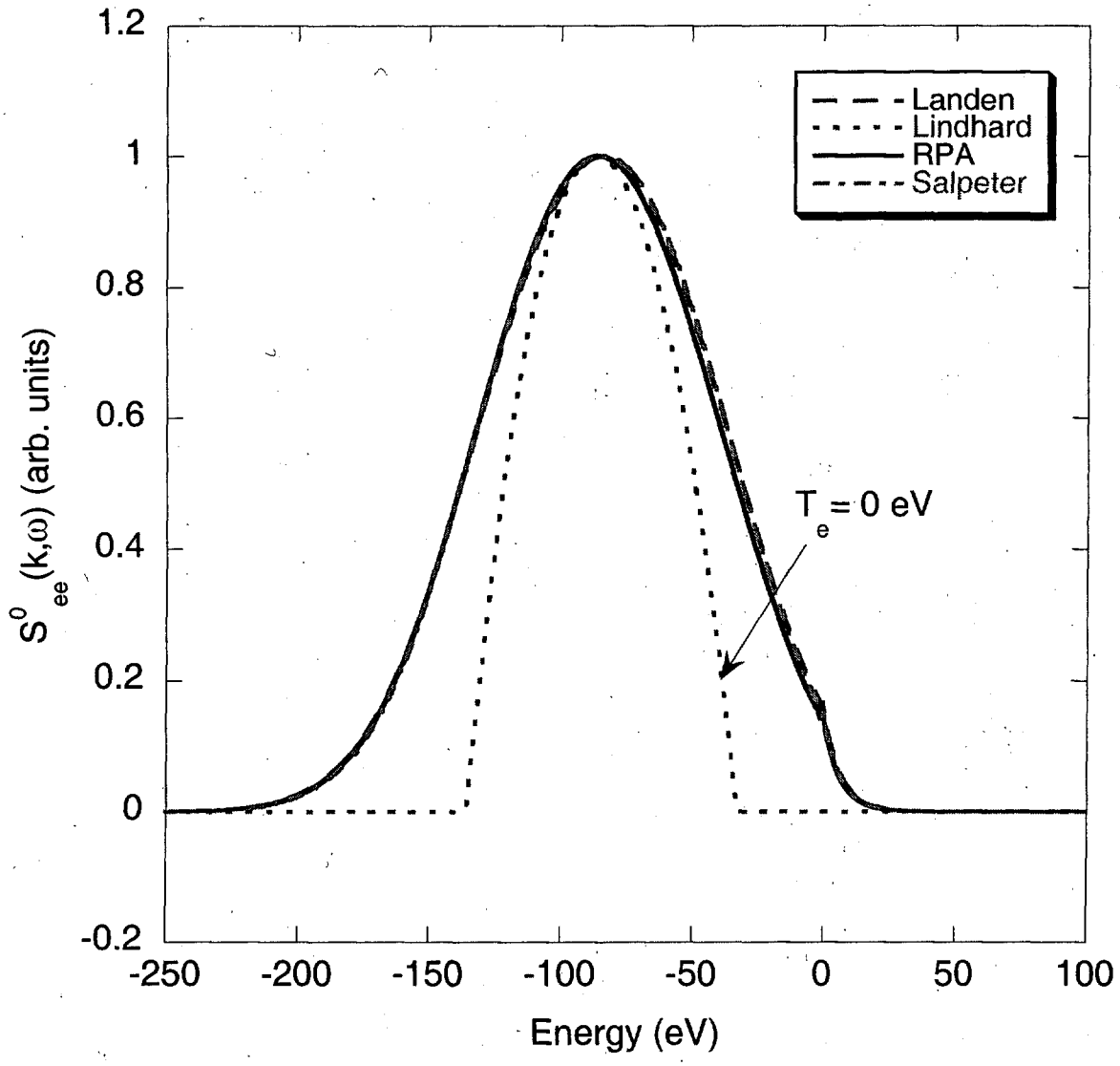
1.2
1
0.8
0.6
0.4
0.2
0
-0.2
-250
-200
-150
-100
-50
0
50
100
Energy (eV)
$S^0_{ee}(k,\omega)$ (arb. units)
Landen
Lindhard
RPA
Salpeter
T_e = 0 eV

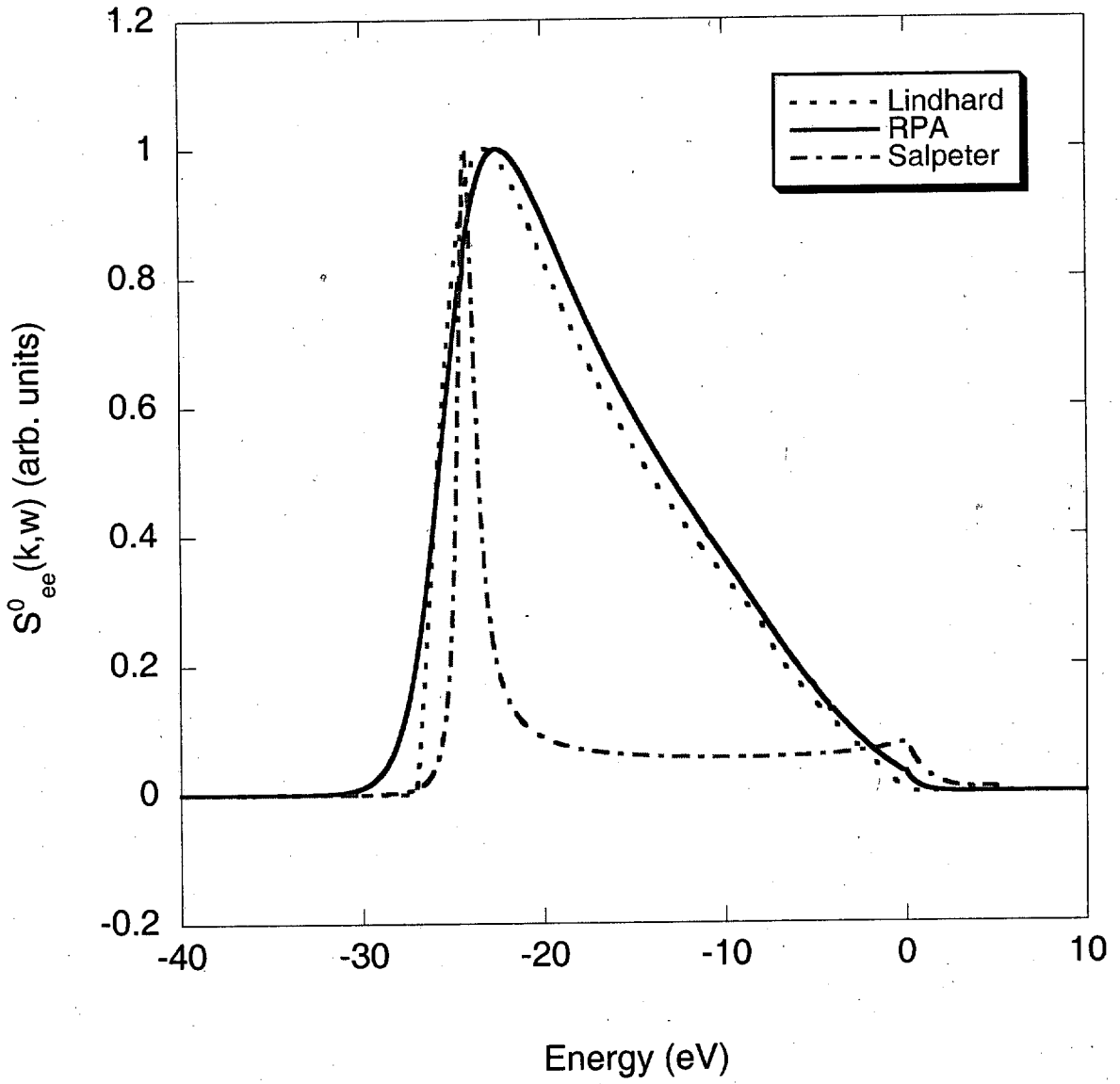
1.2
1
0.8
0.6
0.4
0.2
0
-0.2
-40
-30
-20
-10
0
10
Lindhard
RPA
Salpeter
$S^0_{ee}(k,w)$ (arb. units)
Energy (eV)

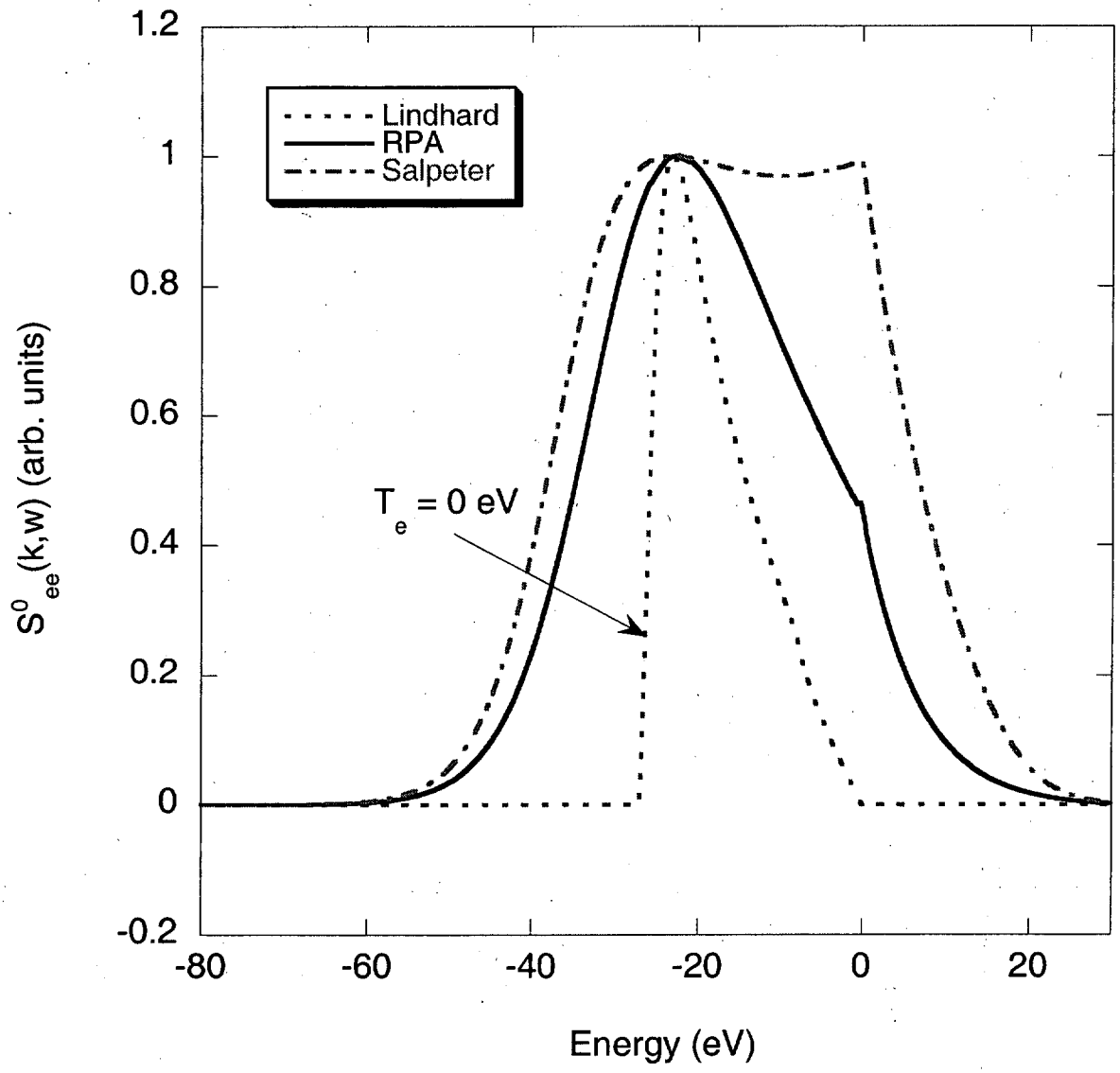
Lindhard
RPA
Salpeter
T_e = 0 eV
$S^0_{ee}(k,w)$ (arb. units)
Energy (eV)
1.2
1
0.8
0.6
0.4
0.2
0
-0.2
-80
-60
-40
-20
0
20

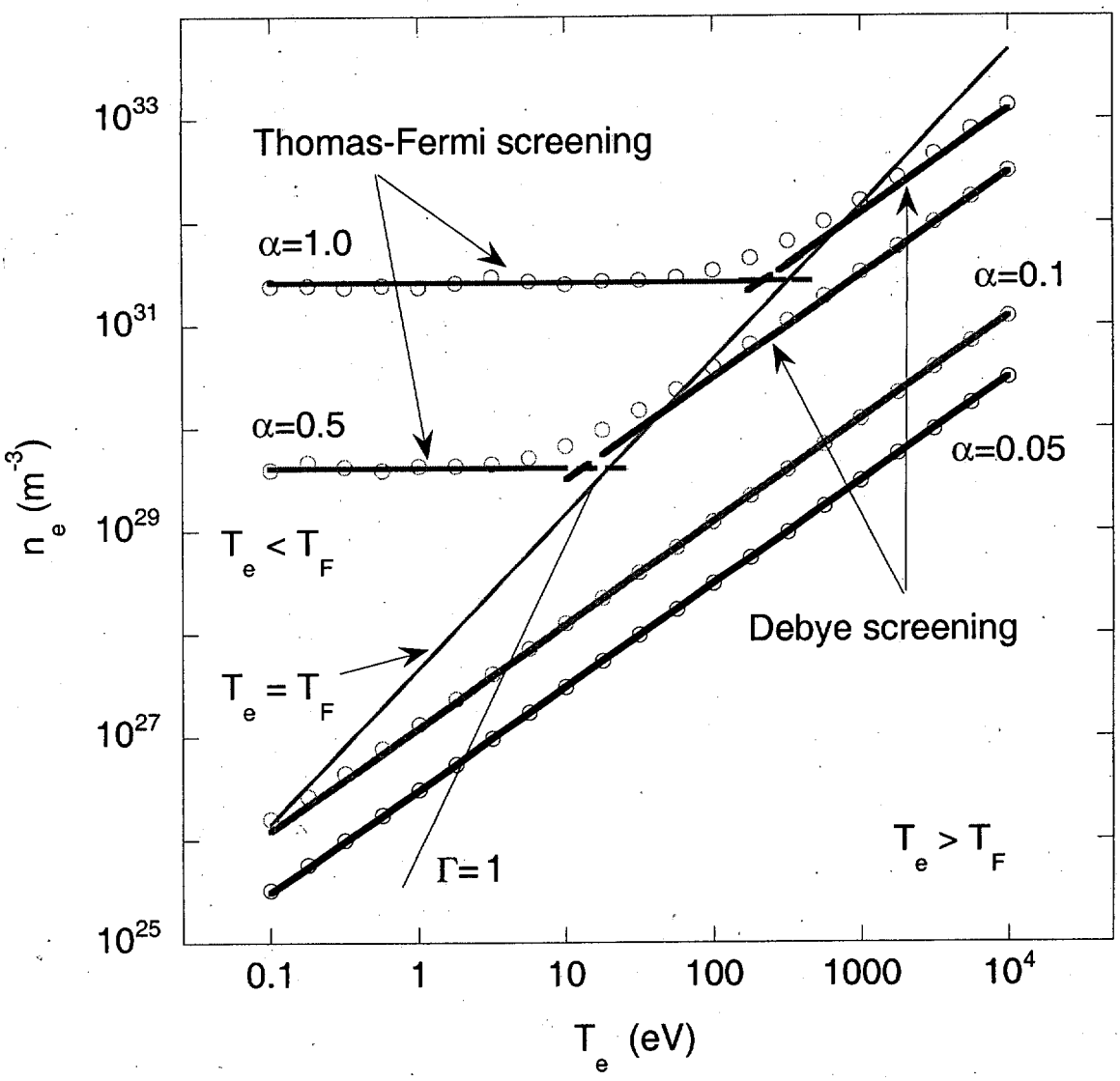
Thomas-Fermi screening
α=1.0
α=0.5
α=0.1
α=0.05
Debye screening
T_e < T_F
T_e = T_F
T_e > T_F
Γ=1
n_e (m^-3)
T_e (eV)
10^33
10^31
10^29
10^27
10^25
0.1
1
10
100
1000
10^4

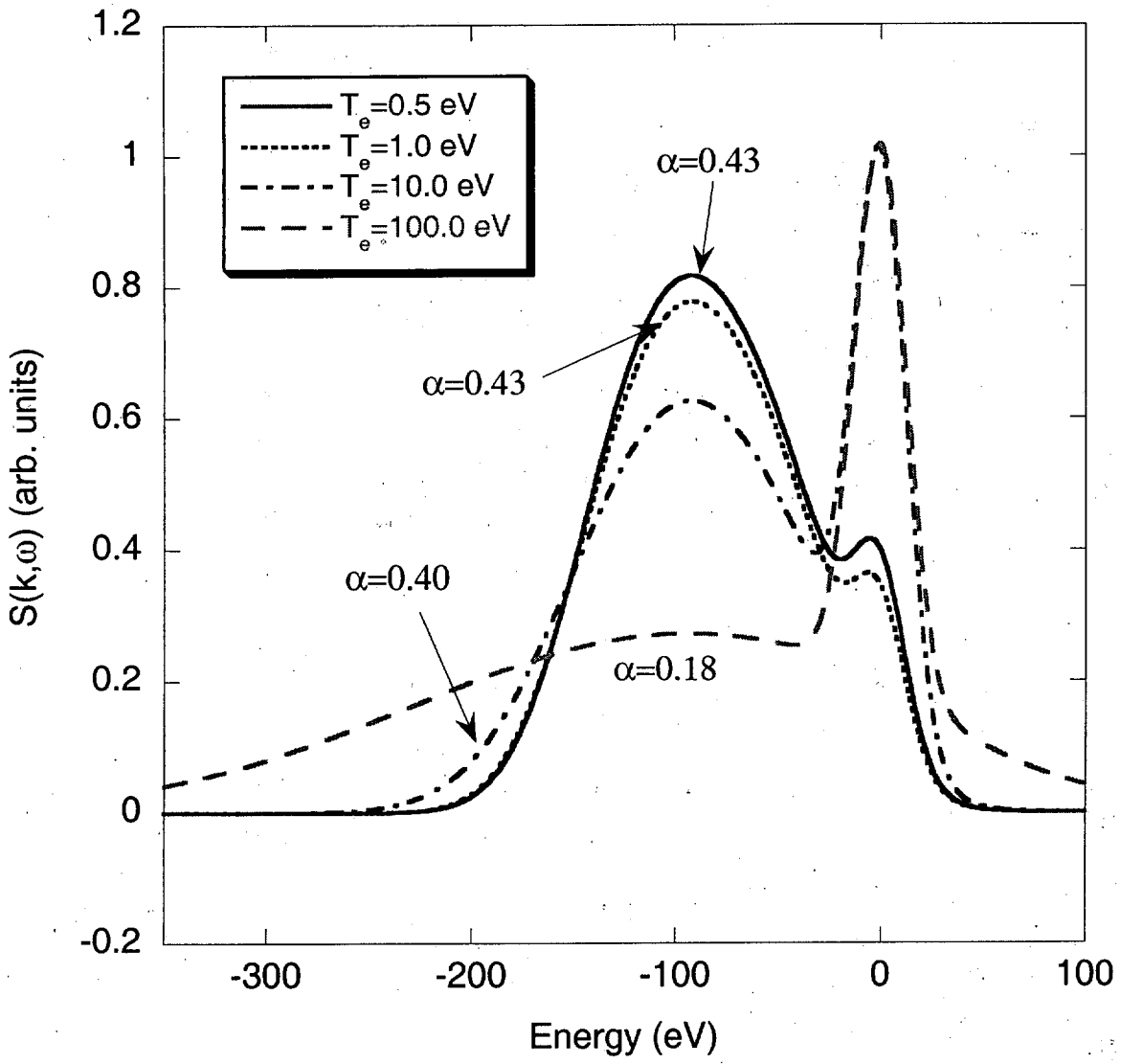
1.2
1
0.8
0.6
0.4
0.2
0
-0.2
S(k,ω) (arb. units)
-300
-200
-100
0
100
Energy (eV)
T_e=0.5 eV
T_e=1.0 eV
T_e=10.0 eV
T_e=100.0 eV
α=0.43
α=0.43
α=0.40
α=0.18

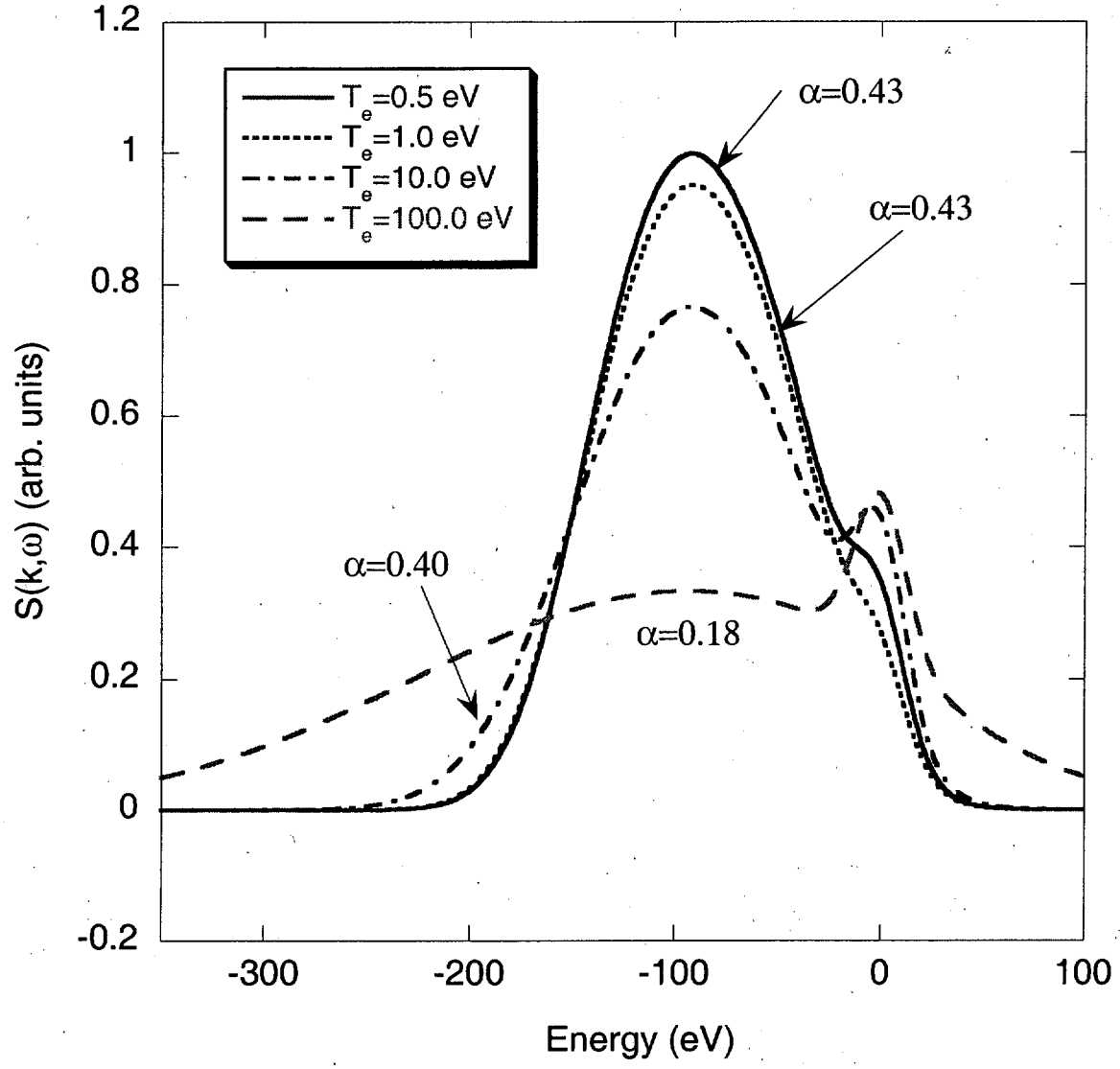
1.2
1
0.8
0.6
0.4
0.2
0
-0.2
S(k,ω) (arb. units)
-300
-200
-100
0
100
Energy (eV)
T_e=0.5 eV
T_e=1.0 eV
T_e=10.0 eV
T_e=100.0 eV
α=0.43
α=0.43
α=0.40
α=0.18